

# Intermodal interference based refractive index sensor employing elliptical core photonic crystal fiber<sup>\*</sup>

WU Xu-jie (吴徐洁)<sup>1</sup>, SONG Bin-bin (宋彬彬)<sup>1\*\*</sup>, WU Ji-xuan (吴继旋)<sup>2</sup>, and HUANG Wei (黄薇)<sup>1</sup>

1. The Key Laboratory of Computer Vision and System of Ministry of Education, Tianjin Key Laboratory of Intelligence Computing and Novel Software Technology, Tianjin University of Technology, Tianjin 300384, China

2. Tianjin Key Laboratory of Optoelectronic Detection Technology and Systems, College of Electronic and Information Engineering, Tiangong University, Tianjin 300387, China

(Received 5 November 2020; Revised 25 November 2020)

©Tianjin University of Technology 2021

A refractive index (RI) sensor based on elliptical core photonic crystal fiber (EC-PCF) has been proposed. The asymmetric elliptical core introduces the polarization-dependent characteristics of the fiber core modes. The performances of intermodal interference between the intrinsic polarization fiber core modes are investigated by contrast in two interferometers based on the Mach-Zehnder (M-Z) and Sagnac interference model. In addition, the RI sensing characteristics of the two interferometers are studied by successively filling the three layers air holes closest to the elliptical core in the cladding. The results show that the M-Z interference between LP<sub>01</sub> and LP<sub>11</sub> mode in the same polarized direction is featured with the incremental RI sensing sensitivity as the decreasing interference length, and the infilled scope around the elliptical core has a weak correlation with the RI sensing sensitivity. Due to the high birefringence of LP<sub>11</sub> mode, the Sagnac interferometer has better RI sensing performance, the maximum RI sensing sensitivity of 12 000 nm/RIU is achieved under the innermost one layer air holes infilled with RI matching liquid of RI=1.39 at the pre-setting EC-PCF length of 12 cm, which is two orders of magnitude higher than the M-Z interferometer with the same fiber length. The series of theoretical optimized analysis would provide guidance for the applications in the field of biochemical sensing.

**Document code:** A **Article ID:** 1673-1905(2021)05-0271-5

**DOI** <https://doi.org/10.1007/s11801-021-0175-6>

Photonic crystal fiber (PCF) is widely used in the field of sensing due to its advantages of abundant light propagating and mode characteristics, flexible structural design, and integration of functional materials<sup>[1-4]</sup>. Nowadays many parameter detections are carried out by employing the excellent performances of PCFs, such as the refractive index (RI)<sup>[5,6]</sup>, external temperature<sup>[7,8]</sup>, strain<sup>[9,10]</sup> and vibration<sup>[11]</sup> etc. Among these parameters the measurement of RI is particularly significant for the biochemical sensing, which benefits from the PCFs' micron order and closed channel for air or fluid infilled, the matter composition and content of analyte infilled in the air holes could be estimated by demodulating the behaviors of modes propagating in the core or cladding.

In recent years, a variety of PCFs have been used for RI sensing. Such as, Tian et al developed a Fabry-Perot cavity based on a concave core PCF for microfluidic RI sensing, which achieved a high RI sensing sensitivity of 1 635.62 nm/RIU around the RI of 1.35<sup>[12]</sup>. Zhao et al

designed and researched the Mach-Zehnder (M-Z) interferometer-based RI sensor realized by adding a PCF with a half-taper folding zone between two single mode fibers (SMF), the RI sensing sensitivity of 181.96 nm/RIU was obtained at the low RI range from 1.333 3 to 1.357 4<sup>[13]</sup>. Luo et al proposed and experimentally verified an RI sensor composed of a SMF-PCF-SMF structure where the air hole of the PCF was filled with alcohol to measure the change of the external RI and the RI sensitivity of 386.66 nm/RIU was obtained in the range of 1.335—1.350<sup>[14]</sup>. Fan et al proposed a PCF-based surface plasmon resonance sensor to achieve an RI sensing sensitivity of 1 931.03 nm/RIU in the RI range from 1.350 to 1.460<sup>[15]</sup>. Most of these reports require introducing complex structures to excite high order cladding modes, in addition, other problems including the low RI sensing responsivity and difficult operation also may become their limitations. Therefore, we propose a design scheme that does not need to excite the cladding mode and only uses the core

<sup>\*</sup> This work has been jointly supported by the Tianjin Natural Science Foundation (No.18JCQNJC71300), the National Natural Science Foundation of China (Nos.11804250, 11904262 and 11704283), the Tianjin Education Commission Scientific Research Project (No.2018KJ146), and the Opening Foundation of Tianjin Key Laboratory of Optoelectronic Detection Technology and Systems (No.2019LODTS004).

<sup>\*\*</sup> E-mail: bbsong@email.tjut.edu.cn

mode that inherently supports transmission for interference sensing. The intermodal interferometers based on birefringent PCF are devised in our work, the phase difference is formed by using different propagation constants of the LP<sub>01</sub> and the LP<sub>11</sub> modes in the fiber core, thereby the RI sensing sensitivity could be estimated through measuring the displacement of the interference spectra. Compared with the interference between the core mode and the excited cladding mode, the LP<sub>01</sub> mode and the LP<sub>11</sub> mode are all intrinsic modes distributed in the fiber core without excitation by complex joint, and the interference between the fiber core modes is more stable owe to they have lower confinement loss when propagating within the PCF core.

In this paper, two RI sensors based on the intermodal interference of elliptic core PCF (EC-PCF) are proposed, the EC-PCF supports polarized LP<sub>01</sub> and LP<sub>11</sub> modes propagating in the core with low confinement loss. The RI sensing performances based on M-Z interferometer and Sagnac interferometer are investigated and compared using the FEM. The theoretical analysis is indispensable guidance for actual RI sensing experimental operation, and our presented sensors have the advantages of compact, stable, high sensitivity and robust, which have broad application prospects in the fields of biochemical sensing.

The cross-sectional view of the designed EC-PCF is shown in Fig.1(a), a germanium-doped elliptic core is introduced into the PCF central area where the RI is 0.004 2 higher than the silica substrate, the semi-major axis and the semi-minor axis are  $a=4.2 \mu\text{m}$ ,  $b=3.5 \mu\text{m}$  respectively. The cladding area of the silica substrate is configured with six layers of air holes arranged in a hexagonal array. These air holes have the uniform diameter of  $d_c=5.2 \mu\text{m}$ , and the pitch of air holes is  $A=8 \mu\text{m}$ , the outer diameter of the silica cladding is designed as  $D=125 \mu\text{m}$  so that it could be well integrated with traditional SMFs to construct robust optical fiber devices. The introduction of the elliptical core enhances the polarization dependent characteristics of PCF, making the effective RI difference between the  $X$  polarization mode and the  $Y$  polarization mode larger. Fig.1(b) shows the effective RI and the birefringence changes of the LP<sub>01</sub> mode and the LP<sub>11</sub> mode in fiber core, it can be seen from the figure that the effective RI of the two modes gradually decreases, while the birefringence between the  $X$  and  $Y$  polarization directions of the modes increases with the wavelength increases, and the birefringence of the LP<sub>11</sub> mode is much larger than the LP<sub>01</sub> mode. The illustration in Fig.1(b) shows the mode field distribution in the  $X$  and  $Y$  polarized directions of the fiber core modes LP<sub>01</sub> and LP<sub>11</sub> simulated by the FEM, due to the boundary limitation of the cladding air holes, most of the optical field energy is concentrated in the elliptical core area, and a small amount of core mode energy is distributed in the form of evanescent field in the air holes of the cladding near the fiber core.

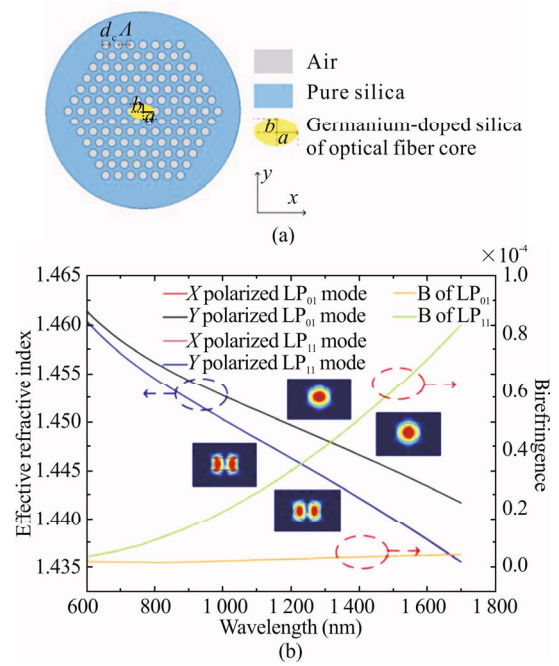


**Fig.1 (a) The cross section view of the proposed EC-PCF; (b) The effective RI curves and birefringence curves of the X and Y polarized LP<sub>01</sub> and LP<sub>11</sub> modes**

When the RI matching liquid is filled in the air holes of the cladding, the light-matter interaction will occur within the evanescent field, and the optical field of the core mode will be modulated at the same time. By demodulating the optical parameter change of the optical field of the core mode, the parameter of the analyte infilled could be sensed, then the RI sensing would be realized. Choosing the fiber core modes LP<sub>01</sub> and LP<sub>11</sub> as the research objects to realize the intermodal interference can greatly improve the optical transmission efficiency while reducing the loss and enhancing the intensity of the optical substance to improve the stability of the interferometer.

In this paper, the EC-PCF RI sensor based on the M-Z interferometer is first modeled theoretically. When the light signal propagates into the EC-PCF, due to the large difference between LP<sub>01</sub> and LP<sub>11</sub>, a phase difference would be accumulated after a certain distance of transmission, which would result in the M-Z intermodal interference. The interference intensity of the LP<sub>01</sub> mode and LP<sub>11</sub> mode could be expressed as follows

$$I=I_1+I_2+2\sqrt{I_1I_2} \cos \varphi , \quad (1)$$

where  $I_1$  and  $I_2$  are the intensities of the LP<sub>01</sub> mode and the LP<sub>11</sub> mode of EC-PCF, and  $\varphi$  is the phase difference between two modes, which could be represented as

$$\varphi=\frac{2\pi\Delta n_{\text{eff}}L}{\lambda} . \quad (2)$$

In the equation,  $L$  is the EC-PCF length, and  $\lambda$  is the wavelength of propagating light,  $\Delta n_{\text{eff}}=n_{\text{eff}}^{\text{LP}_{01}}-n_{\text{eff}}^{\text{LP}_{11}}$  is the effective RI difference between LP<sub>01</sub> and LP<sub>11</sub> modes, according to Eq.(2), when  $\varphi=(2m+1)\pi$ , ( $m=1,2,3,\dots$ ) is the position of the dip of the interference spectrum, the

wavelength is

$$\lambda_m = \frac{2\Delta n_{\text{eff}} L}{2m+1} \quad (3)$$

Therefore, the free space range (*FSR*) of the interference spectrum is

$$FSR = \frac{\lambda^2}{\Delta n_g L} \quad (4)$$

In this equation, the group effective RI difference can be represented as  $\Delta n_g = \Delta n_{\text{eff}} - \frac{d\Delta n_{\text{eff}}}{d\lambda} \lambda$ . According to

Eq.(3),  $\lambda_m$  represents the position of the dip of the *m*-th wave. So the amount of fringe shift can be expressed as

$$\Delta\lambda_m = \frac{2(\Delta n_{\text{eff}} + \Delta n)L}{2m+1} - \frac{2\Delta n_{\text{eff}} L}{2m+1} = \frac{2\Delta n L}{2m+1} \quad (5)$$

In this equation,  $\Delta n$  represents the change of the difference of the effective RI of LP<sub>01</sub> and LP<sub>11</sub>. When the external physical conditions such as RI, temperature, strain, etc. changes,  $\Delta n$  will also change accordingly, which will cause the dip of interference spectrum to shift.

In the Sagnac interferometer model, the incident light splits into two beams respectively from the clockwise and counterclockwise through the EC-PCF, and interferes with each other due to birefringence of the designed EC-PCF. The transmission spectrum intensity can be obtained by the following equation<sup>[16]</sup>

$$P(\text{dBm})=10\lg[1-\cos\varphi]/2, \quad (6)$$

where  $\varphi=2\pi BL/\lambda$  denotes the phase difference, which *B* indicates the birefringence between the *X* and *Y* polarization of LP<sub>11</sub> mode, and *L* is the length of the EC-PCF. When  $BL/\lambda$  is an integer, a dip can be found in the interference spectrum, which could be expressed as

$$\lambda_m = \frac{BL}{m}, (m = 0, \pm 1, \pm 2, \pm 3...) \quad (7)$$

The *FSR* of the interference spectrum is

$$FSR = \frac{\lambda^2}{BL} \quad (8)$$

The *FSR* is affected by fiber birefringence and interference length. As the birefringence or interference length increases, the *FSR* will decrease.

In the M-Z interferometer, the effective RI values of the LP<sub>01</sub> and LP<sub>11</sub> modes obtained by the FEM simulation are taken into Eq.(1), and the interference spectra under the four different EC-PCF lengths of 5 mm, 7 mm, 9 mm and 11 mm are obtained as shown in Fig.2(a). The visible interference spectrum in the figure presents a typical two-beam periodic interference spectrum distribution. As the interference length increases, the *FSR* decreases, which are 110 nm, 78 nm, 62 nm and 51 nm, respectively. This is consistent with the *FSR* of 112.07 nm, 80.05 nm, 62.26 nm and 50.94 nm obtained at 1 560 nm wavelength according to Eq.(4), indicating that the interference spectrum obtained by simulation is in accordance with the theory.

The air holes in the first cladding layer close to the fiber core are selected to fill in to study the influence of different interference lengths on the sensing performance of the infilled liquid analytes. As shown in Fig.2(b), by tracking

the same dip under different RIs, the wavelength shift curves of the interference spectra under different RIs under four interference lengths of 5 mm, 7 mm, 9 mm, and 11 mm are obtained. According to Eq.(3), within the RI range from 1.33 to 1.39, the dip order *m* under four different interference lengths can be obtained as 15, 21, 27 and 33, respectively. Put *m* into Eq.(5) to get the corresponding wavelength shift at different lengths, which are 164.6 nm, 154.3 nm, 147.5 nm and 146.2 nm. The results are consistent with the actual experiment. The RI sensing sensitivity could be observed by taking the derivative of the wavelength shift changes, which are offered in the Tab.1, it shows that the sensitivity decreases with the increase of the interference length under the same RI, which is because the change in effective RI difference is greater than the change in the order on the amount of dips and interference length as Eq.(5). The highest RI sensing sensitivity of 5 200 nm/RIU is achieved under the infilled RI of 1.39 at the EC-PCF length of 5 mm.

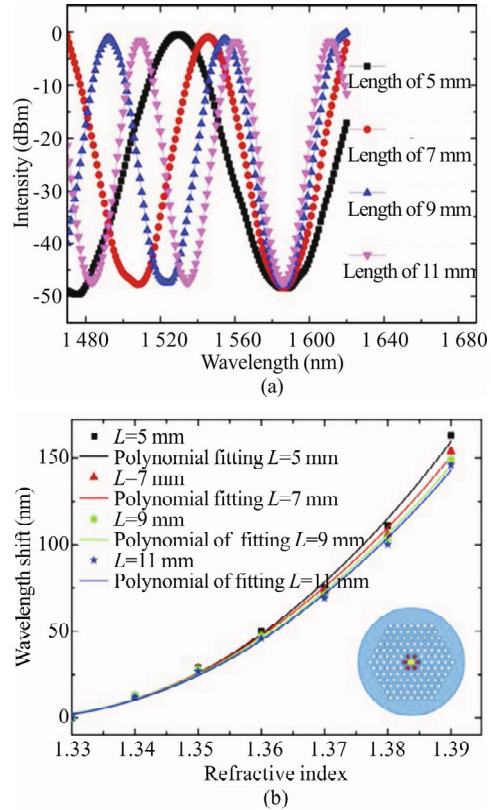


**Fig.2 (a) Interference spectra of the M-Z sensor with different EC-PCF lengths; (b) The wavelength shifts of interference spectra with different EC-PCF lengths**

In order to study the influence of the infilled scope on the RI sensitivity, a layer of air holes (F1), two layers of air holes (F2), and three layers of air holes (F3) close to the fiber core were infilled with the RI range from 1.33 to 1.39 as show in the illustration in Fig.3(a). The RI sensing characteristics of the M-Z interferometer corresponding to the three filling conditions of F1, F2 and F3 are researched. And the corresponding air holes are infilled with RIs ranging from 1.33 to 1.39 at the same interference length

of 5 mm. Fig.3(b) is the effective RI difference figure of the LP<sub>01</sub> and LP<sub>11</sub> modes under different RIs of F1 filling condition, since the effective RI difference under the same analyte RI is almost the same in three cases, only the F1 case is shown here in order to make it clearer observe the change trend of the effective RI difference with the analyte RI. The effective RI decreases with increasing RI infilled so the dips of the interference spectra in the three filling conditions have a red-shift. Fig.3(a) shows the wavelength shift curves of three filling conditions, the wavelength shifts are 164 nm, 167 nm and 167 nm respectively with the RI increase to 1.39. The highest RI sensing sensitivity is 5 400 nm/RIU when RI is 1.39 and infilled with F2 and F3. In brief, the RI sensing sensitivity changes little under these three filling conditions, indicating that the infilled scope is farther away from the fiber core, the smaller the impact on the core mode of the fiber, in other words, for the F1 filling situation, only filling the layer of air holes closest to the fiber core can achieve high RI sensing sensitivity. In the field of biosensing, it greatly reduces the consumption of the analytes.

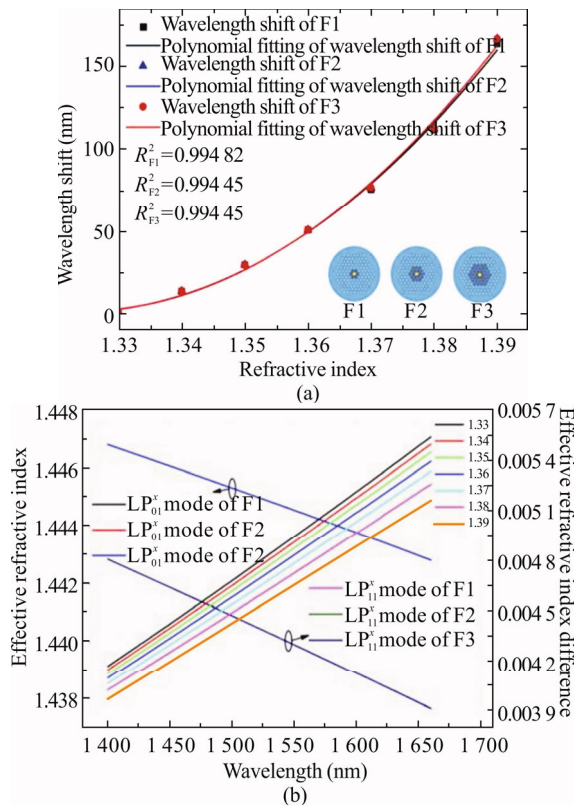


**Fig.3 (a) The wavelength shifts of F1, F2, F3 three filling conditions; (b) The effective RI curves of LP<sub>01</sub> and LP<sub>11</sub> modes under F1, F2, F3 conditions, and the effective RI difference curves of F1**

The RI sensing performances are compared between the Sagnac interferometer and the M-Z interferometer. Due to the low ellipticity of the elliptical core introduced in EC-PCF, the birefringence of LP<sub>01</sub> mode is an order of magnitude smaller than that of LP<sub>11</sub> mode as presented in Fig.1(b), which results in difficulty in the demodulation

of tracking responses of interference spectrum. Therefore, the LP<sub>11</sub> mode with higher birefringence is selected as candidate to observing Sagnac interference spectrum. In order to present a complete interference period in the operating wavelengths range from 600 nm to 1 700 nm, the interference length of two interferometers are set to 12 cm, and employing F1 filling method with RI range from 1.33 to 1.39. The interference spectra in two interferometers are obtained as shown in Fig.4(b), the FSR of the Sagnac interference spectrum is about 185.5 times of that of the M-Z interference spectrum.

The interference spectra of the Sagnac interferometer in Fig.4(b) have red shifts as the RI of the infilled liquid increases, because as the RI increases, the birefringence between the two orthogonal polarized LP<sub>11</sub> modes in Fig.4(a) increases at the same wavelength. The black curve in Fig.4(b) is the wavelength shift curve of the Sagnac interference, with the infilled RI increase up to 1.39, the wavelength shifts reach up to 320 nm, and the highest sensitivity of 12 000 nm/RIU is achieved.

The M-Z interference spectra in Fig.4(b) are under the same condition. The wavelength shift curve is observed through calculating and tracking the 282th-order dip A at the wavelength of 984.9 nm, as presented in the red curve of Fig.4(b), which only achieving red shifts of 32.8 nm over the RI range from 1.33 to 1.39. The RI sensing sensitivity of the M-Z interferometer is two orders of magnitude lower than that of the Sagnac interferometer, which indicates that the EC-PCF-based Sagnac interferometer possesses the optimal RI sensing performance.

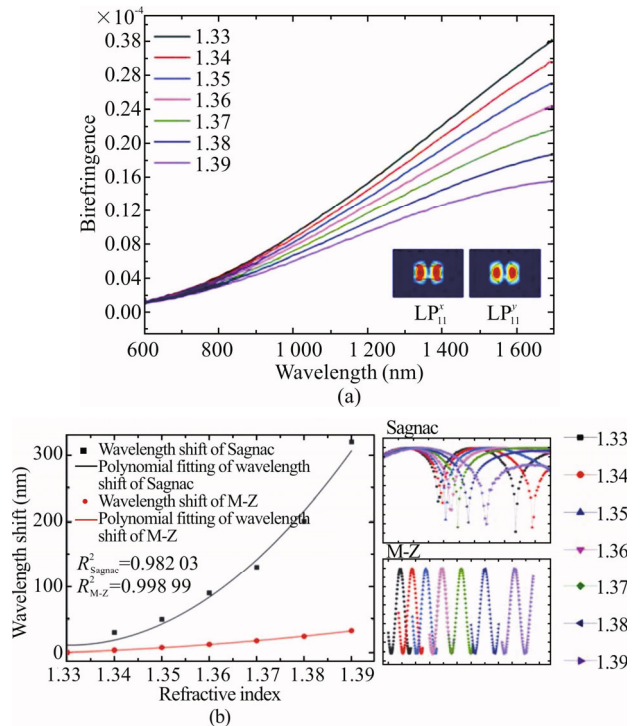


**Fig.4 (a) The birefringence curves of the LP<sub>11</sub> mode under different RI ranging from 1.33 to 1.39; (b) The wavelength shifts of Sagnac and M-Z interference spectra**

**Tab.1 The RI sensing sensitivities of M-Z and Sagnac interferometers**

$n_a$		1.33	1.34	1.35	1.36	1.37	1.38	1.39	
RI sensitivity of M-Z (nm/RIU)	$L$	5 mm	1 400	1 500	1 850	2 300	3 050	4 400	5 200
		7 mm	1 300	1 450	1 750	2 200	2 900	4 050	4 800
		9 mm	1 300	1 400	1 700	2 100	2 750	3 950	4 700
		11 mm	1 200	1 350	1 700	2 100	2 700	3 850	4 600
		12 cm	340	365	425	510	615	765	860
	Filling method	F1	1 400	1 500	1 850	2 300	3 050	4 400	5 200
	F2	1 400	1 500	1 850	2 350	3 100	4 500	5 400	
	F3	1 400	1 500	1 850	2 350	3 100	4 500	5 400	
RI sensitivity of Sagnac (nm/RIU)	$L=12$ cm	3 000	3 000	3 000	4 000	6 000	9 000	12 000	

In this paper, a high-sensitivity RI sensor based on EC-PCF has been designed and investigated. Due to the polarization characteristics of the elliptical core, the FEM has been used to study and compare the interference characteristics of the M-Z interferometer and the Sagnac interferometer. In the M-Z interferometer, the increase of the infilled scope has almost no effect on the sensitivity. The results show that when the RI is 1.39 and the interference length is 5 mm, the RI sensitivity of 5 200 nm/RIU is obtained when first layers of air holes are filled. And when the interference length increased to 12 cm, due to the high birefringence of LP<sub>11</sub> mode, Sagnac interferometer showed a higher sensitivity of 12 000 nm/RIU at an RI of 1.39, which is two orders of magnitude higher than the M-Z interferometer with the same length. The sensor could be further studied in biomedical and environmental detection fields.

## References

- [1] Yuan T, Yang X, Liu Z, Yang J, Li S, Kong D, Qi X, Long Q and Yuan L, *Optics Express* **25**, 18205 (2017).
- [2] Xing Z, Wang Y, Tang L, Yu J, Guan H, Lu H, Fang J, Luo Y, Zhong Y and Chen Z, *Optical Fiber Technology* **50**, 13 (2019).
- [3] Andrews N L P, Ross R, Munzke D, Van Hoom C, Brzezinski A, Barnes J A, Reich O and Look P, *Optics Express* **24**, 14086 (2016).
- [4] Zhang N, Humbert G, Wu Z, Li K, Shum P P and Zhang N M Y, *Optics Express* **24**, 27674 (2016).
- [5] Zhao Y, Li X G, Cai L and Yang Y, *Sensors & Actuators B Chemical* **221**, 406 (2015).
- [6] Chen C H, Wu W T and Wang J N, *Technologies* **23**, 1 (2016).
- [7] Monfared Y E, Ahmadian A, Dhasarathan V and Liang C, *Photonics* **7**, 33 (2020).
- [8] Lv L, Liu Q and Xue P, *Results in Physics* **18**, 103198 (2020).
- [9] Tian J, Jiao Y, Fu Q, Ji S, Li Z, Quan M and Yao Y, *Journal of Lightwave Technology* **36**, 1 (2018).
- [10] Han T, Liu Y and Wang Z, A High Sensitivity Strain Sensor Based on a Selective-Filling High Birefringent Photonic Crystal Fiber Sagnac Interferometer, 2017 Conference on Lasers and Electro-Optics Pacific Rim (CLEO-PR), 2017.
- [11] Yu H, Luo Z, Zheng Y, Ma J, Li Z and Jiang X, *Journal of Lightwave Technology* **37**, 2261 (2019).
- [12] Tian J, Lu Z, Quan M, Jiao Y and Yao Y, *Optics Express* **24**, 20132 (2016).
- [13] Zhao Y, Xia F, Hu H F and Chen M Q, *Optics Communications* **402**, 368 (2017).
- [14] Luo Y, Fan R, Zhang Y, Wu Q, Ren Z and Peng B, *Optical Fiber Technology* **48**, 278 (2019).
- [15] Guo Z P, Fan Z, Kong X Z and Meng Z Y, *Optics Communications*, 461 (2020).
- [16] Ma M J, Chen H L, Li S G, Zhang W X, Liu Y C and Zhu E K, *Optik International Journal for Light & Electron Optics*, 179 (2018).